Atomic-Scale Heterogeneity of a Multicomponent Bulk Metallic Glass with Excellent Glass Forming Ability

T. Fujita,[1] K. Konno,[2] W. Zhang,[3] V. Kumar,[3] M. Matsuura,[2] A. Inoue,[1,3] T. Sakurai,[1] and M. W. Chen[1,3,*]

[1]*WPI Advanced Institute for Materials Research, Tohoku University, Sendai 980-8577, Japan*

[2]*Miyagi National College of Technology, Natori 981-1239, Japan*

[3]*Institute for Materials Research, Tohoku University, Sendai 980-8577, Japan*

(Received 30 July 2008; published 12 August 2009)

We report the atomic structure of a multicomponent $Cu_{45}Zr_{45}Ag_{10}$ bulk metallic glass investigated by state-of-the-art experimental and computational techniques. In comparison with a binary $Cu_{50}Zr_{50}$ metallic glass, Zr-rich interpenetrating clusters centered by paired and stringed Ag atoms and Cu-rich icosahedra are widely observed in the ternary $Cu_{45}Zr_{45}Ag_{10}$ alloy. The atomic-scale heterogeneity caused by chemical short- and medium-range order is found to play a key role in stabilizing the liquid phase and in improving the glass forming ability of the multicomponent alloy.

DOI: 10.1103/PhysRevLett.103.075502 PACS numbers: 61.43.Fs, 61.05.cj, 61.43.Dq

Formation mechanisms of multicomponent bulk metallic glasses (BMGs) with very low critical cooling rates have been one of the most outstanding issues in solid-state physics and materials science [1–3]. In general, the formation and stability of condensed matter are closely related to their atomic structure. Nevertheless, the structure of BMGs is poorly known and, as a result, the atomic origins of the glass forming ability (GFA) of BMGs have not been well understood [4–7]. Historically, Bernel's dense random packing model has been widely used to explain the atomic structure of metallic glasses in which the atomic arrangements are considered from purely geometrical sphere packing [8]. However, this model fails to explain short-range orders (SROs) and medium-range orders (MROs) that are frequently observed in multicomponent glassy systems. Recently, efficient atomic packing with the schemes of overlapping of solute-centered atomic clusters and ''quasiequivalent'' solute-centered atomic clusters [4,9,10] has been suggested as the structures of amorphous alloys. The validity of these cluster models has been verified by a number of binary metallic glasses. It has been found that atomic size ratios of constituent elements are the most important factor governing GFA, particularly in alloys only containing transition metals, which is consistent with traditional glass forming theories [2,11]. However, the atomic structures of BMGs with multiple components and excellent GFA have not been well investigated and the chemical effects arising from interatomic interactions in the multicomponent systems have not been comprehensively assessed [4,9,10,12].

An interesting phenomenon in BMGs is that selective minor additions can dramatically improve the GFA of binary metallic glasses [13]. For example, the addition of 10 at. % Ag to a $Cu_{50}Zr_{50}$ BMG can obviously improve the GFA and leads to the increase of critical sample diameters from ~2 to ~6 mm [14]. However, the improved GFA appears to conflict with the current understandings in BMG formation because the positive heat of mixing (2 kJ/mol) for the Cu-Ag pair [15] is empirically expected to degrade the GFA of the resultant $Cu_{45}Zr_{45}Ag_{10}$ alloy [2]. In this study, the atomic structure of the ternary $Cu_{45}Zr_{45}Ag_{10}$ BMG was investigated by using extended x-ray absorption fine structure (EXAFS) spectroscopy combining with *ab initio* molecular-dynamics (MD) simulations. We aim to elucidate the atomic origins of the improved GFA of the multicomponent BMG.

Three glassy alloys, $Cu_{50}Zr_{50}$, $Cu_{45}Zr_{45}Ag_{10}$, and $Cu_{40}Zr_{40}Ag_{20}$ (at. %), prepared by a melt-spinning method, were used in this study. The atomic structures of the BMGs were investigated by EXAFS spectroscopy at the beam line BL01B1 of the SPring-8 synchrotron radiation facility, Japan. EXAFS spectra of Cu-*K*, Zr-*K* and Ag-*K* edges were measured in a transmission mode at a temperature of 20 ± 0.1 K. The thicknesses of the samples were optimized to obtain suitable absorption jumps at each *K*-absorption edge. The experimental EXAFS signals were extracted by a standard data-reduction procedure using the UWXAFS program [16]. Independent computational simulations of the atomic structures of $Cu_{50}Zr_{50}$, $Cu_{45}Zr_{45}Ag_{10}$, and $Cu_{40}Zr_{40}Ag_{20}$ were performed using the Vienna *ab initio* simulation package (VASP) [17]. The atoms were arranged in a cubic box with periodic boundary conditions. Each configuration with a known density [18,19], consisting of approximately 250 atoms, was melted at 2500 K for a total of 2000 steps with each step time of 5 fs. Subsequently, the systems were quenched to 300 K with a cooling rate of $\sim 4 \times 10^{13}$ K s^{-1} at 1000 time steps per 200 K. The temperatures were controlled using the Nose-Hoover thermostat and the final configurations were obtained using a conjugated gradient method [20]. The EXAFS spectra $\chi_{\mathrm{model}}(k)$ of the simulated atomic configurations were calculated using an *ab initio* code implanted in FEFF8 [21].

Figures 1(a) and 1(b) show the experimental EXAFS spectra $k^2\chi(k)$ of Cu-*K* and Zr-*K* edges of glassy $Cu_{50}Zr_{50}$, $Cu_{45}Zr_{45}Ag_{10}$, and $Cu_{40}Zr_{40}Ag_{20}$ alloys, respectively. The

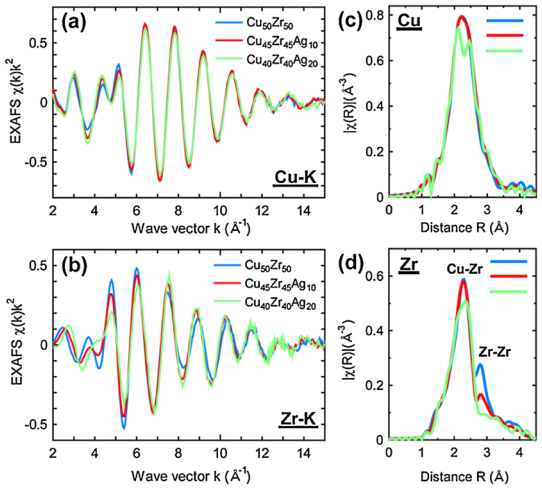

FIG. 1 (color online). Experimental EXAFS spectra from glassy $Cu_{50}Zr_{50}$, $Cu_{45}Zr_{45}Ag_{10}$ and $Cu_{40}Zr_{40}Ag_{20}$ alloys. (a) and (b) EXAFS spectra $k^2\chi(k)$ of $Cu_{50}Zr_{50}$, $Cu_{45}Zr_{45}Ag_{10}$, and $Cu_{40}Zr_{40}Ag_{20}$ for Cu-K and Zr-K, respectively; (c) and (d) The Fourier transforms of the Cu-K and Zr-K edges from $Cu_{50}Zr_{50}$, $Cu_{45}Zr_{45}Ag_{10}$ and $Cu_{40}Zr_{40}Ag_{20}$, respectively.

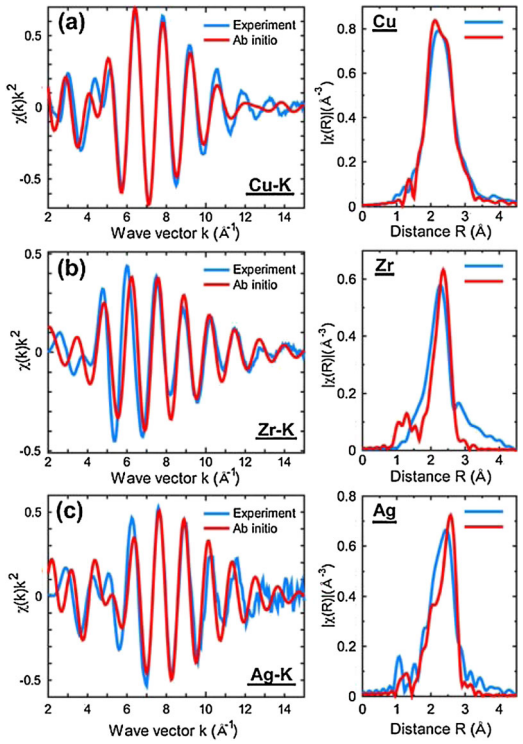

FIG. 2 (color online). EXAFS spectra $k^2\chi(k)$ of $Cu_{45}Zr_{45}Ag_{10}$ and corresponding Fourier transforms at (a) Cu-K, (b) Zr-K, and (c) Ag-K edges obtained experimentally (blue lines) and by model calculations using 300 K *ab initio* configuration (red lines).

spectra of the $Cu_{50}Zr_{50}$ and $Cu_{45}Zr_{45}Ag_{10}$ at the Cu-K edge exhibit nearly identical features, indicating that the addition of 10 at. % Ag does not induce detectable changes in the nearest neighbors of Cu atoms. However, noticeable peak splitting appears at the Cu-K edge of $Cu_{40}Zr_{40}Ag_{20}$, indicating possible phase separation [22]. The spectra of the samples at the Zr-K edge show obvious changes with Ag addition, particularly in the low-k region. Fourier transform of the Zr-K edge spectra suggests that the dissimilarity among the BMGs is associated with the disparity in the magnitude of the peaks corresponding to Zr-Zr interatomic pairs [Fig. 1(d)]. Because the peak magnitude is related to the number of neighboring atoms [23], considering the inconspicuous difference in the Fourier transformed Cu-K edges between $Cu_{50}Zr_{50}$ and $Cu_{45}Zr_{45}Ag_{10}$ [Fig. 1(c)], we can deduce that the addition of Ag results in the selective replacement of a portion of the Zr-Zr pairs by Zr-Ag pairs.

Figures 2(a)–2(c) shows the experimental and calculated EXAFS spectra of $Cu_{45}Zr_{45}Ag_{10}$ at Cu-K, Zr-K and Ag-K edges. The spectral features of the simulated $\chi_{\mathrm{model}}(k)$ fairly match with those of the experimental spectra, although there is a slight discrepancy (smaller than 5%) in the interatomic distances of Zr-Cu and Zr-Ag [Fig. 2(b) and 2(c)]. Reasonable agreement between the experimental and computational EXAFS spectra is also achieved in the $Cu_{50}Zr_{50}$ and $Cu_{40}Zr_{40}Ag_{20}$ systems (see the supplementary material [24]). Therefore, the atomic configurations predicted by the independent VASP simulations are fairly consistent with the primary structures of the real alloys, from which we can search dominant polyhedra in the glassy alloys using a Voronoi tessellation method [25]. With Zr atoms as the solute centers, a preferred polyhedron cannot be found in the alloys [Fig. 3(b)], suggesting that Zr atoms most likely reside in the shells of solute-centered clusters. In contrast, preferred polyhedra with high frequency fractions appear when Cu and Ag are chosen as the solute atoms [Figs. 3(c) and 3(d)]. The leading topological SRO for both alloys is an icosahedronlike cluster with a Voronoi index of $\langle 0281 \rangle$, which has been proved to be a favorable building unit for good glass formers because of the efficient atomic packing and energy minimization [5,10]. It is worth noting that the icosahedronlike clusters become more prominent in $Cu_{45}Zr_{45}Ag_{10}$ than in $Cu_{50}Zr_{50}$ and $Cu_{40}Zr_{40}Ag_{20}$ [Fig. 3(c)], demonstrating that 10 at. % Ag addition improves the packing efficiency. From topological point of view, atomic packing efficiency is closely related to the effective atomic size ratio between the solute and solvent atoms and the ratio close to 0.902 can produce the most efficient atomic packing with icosahedronlike clusters as the predominant SROs. [4,5,9,10,12] Although the 10 at. % Ag addition can slightly increase the effective atomic size ratio of $\boldsymbol{R_{Cu}/R_{Zr}}$ from 0.8806 to 0.8809 calculated by the nominal alloy compositions, it may not be the major reason leading to the dramatically improved GFA because of the fact that further adjusting the Ag concentration to 20 at. % can increase the effective atomic size ratio to 0.8813 whereas results in the loss of the GFA [14].

We noticed that the distribution of the constituent elements in the simulated atomic structures of $Cu_{45}Zr_{45}Ag_{10}$ and $Cu_{40}Zr_{40}Ag_{20}$ is inhomogeneous and more than 90%

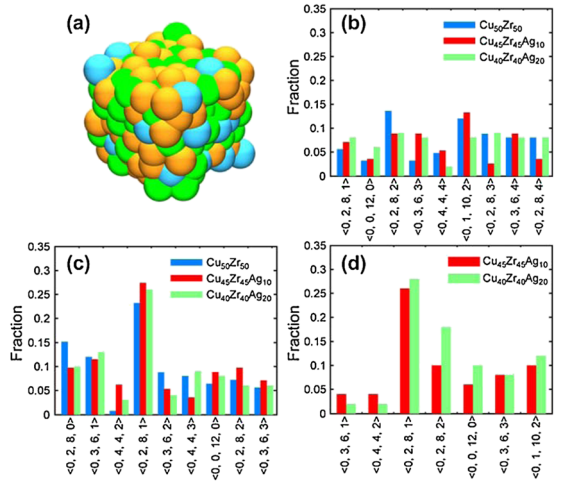

FIG. 3 (color online). (a) 3D atomic configuration of $Cu_{45}Zr_{45}Ag_{10}$ predicted by *ab initio* MD simulations. The bronze, green and light blue balls represent Cu, Zr, and Ag atoms, respectively. (b) The fraction of dominant polyhedra centered by Zr atoms, (c) Cu atoms, and (d) Ag atoms. The blue, red, and green bars represent the results of $Cu_{50}Zr_{50}$, $Cu_{45}Zr_{45}Ag_{10}$, and $Cu_{40}Zr_{40}Ag_{20}$, respectively, and the polyhedra are indexed by Voronoi indices.

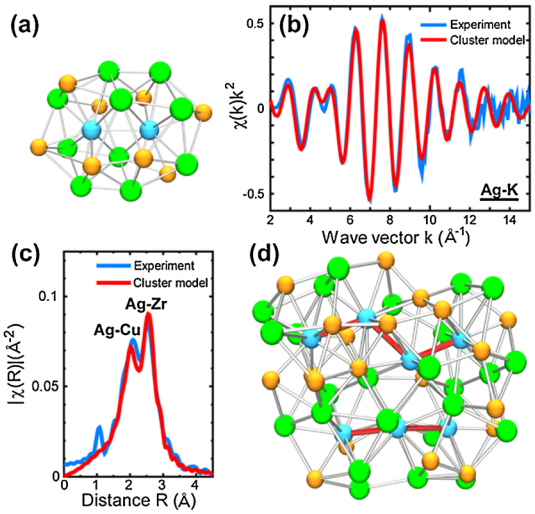

FIG. 4 (color online). Ag-centered interpenetrating cluster and corresponding EXAFS spectra. (a) An interpenetrating cluster with paired Ag atoms in the center; (b) EXAFS spectra $k^2\chi(k)$ of Ag-K edges from experiment and from the interpenetrating cluster shown in (a); (c) Fourier transform of Ag-K edge EXAFS spectra $k\chi(k)$; and (d) a large interpenetrating clusters centered by stringed Ag atoms. The red line denotes Ag-Ag connections, and the bronze, green, and light blue balls represent Cu, Zr, and Ag atoms, respectively.

of the Ag atoms are in the form of Ag atom pairs and strings. Quantitative analysis shows that the coordination number of Ag atoms in $Cu_{45}Zr_{45}Ag_{10}$ ranges from 10 to 13. The averaged value is 11.5, which consists of 3.9 Cu, 6.2 Zr, and 1.4 Ag atoms, indicating that on average each Ag atom has at least one Ag atom as its nearest neighbor. The fact that Ag atoms have more Zr and fewer Cu atoms as the nearest neighbors than those expected from the alloy composition is also consistent with the EXAFS results in which Zr-Zr pairs are selectively replaced with Zr-Ag pairs. Additionally, the atomic-scale heterogeneity with the formation of Zr-rich clusters centered by Ag pairs and strings also causes that the Cu-centered clusters contain more Cu and lesser Zr, resulting in the effective atomic size ratio of Cu center clusters of ~0.901, very close to the ideal value (0.902) for the most efficient atomic packing.

We selected a representative interpenetrating cluster centered by paired Ag atoms [Fig. 4(a)] and confirmed that the number of coordinated atoms surrounding each Ag atom in the cluster is close to the average values measured by the quantitative Voronoi analysis [25]. The position of each atom in the cluster was optimized by *ab initio* MD calculations with an allowed displacement of less than 0.06 Å. The Ag K-edge EXAFS spectrum of the interpenetrating cluster was calculated and compared with the experimental data [Fig. 4(b)]. It shows that the spectrum of the cluster pair has better agreement with the experimental one than that from the simulated structure containing the entire 251 atoms [Fig. 2(c)]. Except very small difference (~0.03 Å) in the Ag-Cu pair, the nearly identical features, especially in the low-k region and at the Ag-Zr peak [Figs. 4(b) and 4(c)] strongly supports that the interpenetrating cluster is the predominant polyhedron for Ag-centered clusters in the real $Cu_{45}Zr_{45}Ag_{10}$ BMG. Apparently, the very low cooling rate (~10^6 Ks^{-1}) of the glassy ribbons produced by melt spinning allows more pronounced and well-developed SROs and MROs than the simulated glass with a high cooling rate (~4×10^{13} Ks^{-1}). In addition to the paired Ag atoms, atomic strings consisting of three or four Ag atoms are also observed in the simulated structure, which forms a large atomic cluster through interpenetration of three or four Ag-centered icosahedrons—like polyhedra [Fig. 4(d)]. This atomic-scale heterogeneity can be well reproduced by VASP simulations using different initial configurations and by conventional MD simulations with 8000 atoms and much slower cooling rate (2×10^{10} K/s) (see the supplementary material [24]). It is worth noting that the extent of the heterogeneity in $Cu_{40}Zr_{40}Ag_{20}$ increases by the percolation of extended Ag-rich clusters (see the supplementary material [24]), which leads to the nanoscale phase separation that is consistent with the peak splitting shown in the EXAFS spectrum (Fig. 1).

From the kinetic point of view, the formation of BMGs is a competition process between supercooling liquid phase and crystallization [26]. As an empirical rule, the most appropriate compositions for glass formation are those that stabilize the liquid phases relative to crystalline phases. For $Cu_{45}Zr_{45}Ag_{10}$, we analyzed the atomic configuration in the liquid state and the evolution of the chemical order during the quenching. The results clearly indicate that the chemical heterogeneity also appears in the liquid alloy and the Ag-centered interpenetrating clusters

are still the preferred SROs and MROs (~80% Ag atoms in the forms of pairs and strings). Similar to simple icosahedra, the interpenetrating clusters lack translational periodicity and have difficulty in growth in comparison with the crystal counterparts. Moreover, the atomic-scale chemical heterogeneity with the formation of Ag pairs and strings also leads to the Cu-centered clusters with fewer Zr and more Cu, deviating from the statistic average of the alloy composition. Although the effective atomic size ratio calculated from the nominal composition of the alloy may not satisfy the ideal value for effective atomic packing, the local composition of individual clusters in the alloy may have an effective atomic ratio close to the ideal value because of the atomic-scale chemical heterogeneity. Different from the traditional viewpoint that atoms typically prefer to be surrounded by unlike atoms and atomic packing is based on the statistical average of the alloy compositions, the observations of the chemical effect and resultant atomic-scale heterogeneity apparently revise the previously empirical understandings about bulk glass formation and provide microscopic understanding on GFA. Combining with the recent works on dynamic heterogeneity in glassy materials [27,28], we believe that the atomic-scale heterogeneity caused by the chemical effect, which has been ignored in traditional models of metal-metal based metallic glasses, plays an important role in GFA of multicomponent alloys.

Historically, the chemical SROs and MROs have been proposed as structure units of glassy metal-metalloid alloys in light of the strong chemical affinity between metal and metalloid elements [29]. However, chemical SROs and MROs in metal-metal based metallic glasses, particularly in multicomponent BMGs, have not been well elucidated before, although it has been noticed that the good glass formers generally have negative heats of mixing among the main constituent elements [2]. Obviously, the interpenetrating clusters and atomic-scale chemical heterogeneity observed in this study are intrinsically different from the traditional chemical SROs and MROs formed by strong chemical affinity between constituent elements [29]. Interestingly, the chemical order in the $Cu_{45}Zr_{45}Ag_{10}$ BMG is caused by the addition of an immiscible element and not by enhancing chemical affinity. The unexpected chemical SROs and MROs are unambiguously associated with the multicomponent effect; i.e., chemical heterogeneity provides more opportunities to form atomic combinations with both efficient atomic packing and energy minimization for individual clusters. Apparently, over a certain extent, for example, of $Cu_{40}Zr_{40}Ag_{20}$, the chemical heterogeneity may result in strong chemical segregations and even phase separation which thereby reduces GFA.

In summary, we have studied the atomic structure of a multicomponent $Cu_{45}Zr_{45}Ag_{10}$ BMG by using EXAFS spectroscopy and *ab initio* MD simulations. The good GFA of the alloy is found to be associated with the atomic-scale chemical heterogeneity by the formation of Zr-rich interpenetrating clusters centered by Ag atom pairs and strings and Cu-centered icosahedral polyhedra with enriched Cu. This finding has elucidated the importance of interatomic interactions and chemical heterogeneity in the formation of multicomponent BMGs with excellent GFA.

We thank Dr. Howard Sheng for help in the MD simulations. This work is sponsored by ''Global COE for Materials Research and Education'' and ''World Premier International Research Center Initiative'', MEXT, Japan. The EXAFS experiments are supported by the JASRI/SPring-8 under Proposal Number 2007B1346, 2008A1482, and 2008B1336.

*Corresponding author.
mwchen@wpi-aimr.tohoku.ac.jp

[1] A. L. Greer, Nature (London) **366**, 303 (1993).
[2] A. Inoue, Acta Mater. **48**, 279 (2000).
[3] W. L. Johnson, MRS Bull. **24**, 42 (1999).
[4] D. B. Miracle, Nature Mater. **3**, 697 (2004).
[5] X. K. Xi, L. L. Li, B. Zhang, W. H. Wang, and Y. Wu, Phys. Rev. Lett. **99**, 095501 (2007).
[6] M. W. Chen, Annu. Rev. Mater. Res. **38**, 445 (2008).
[7] F. Delogu, Phys. Rev. Lett. **100**, 075901 (2008).
[8] J. D. Bernal, Nature (London) **185**, 68 (1960).
[9] D. B. Miracle, Acta Mater. **54**, 4317 (2006).
[10] H. W. Sheng, W. K. Luo, F. M. Alamgir, and E. Ma, Nature (London) **439**, 419 (2006).
[11] T. Egami and Y. Waseda, J. Non-Cryst. Solids **64**, 113 (1984).
[12] H. Ruppersberg, D. Lee, and C. N. J. Wagner, J. Phys. F **10**, 1645 (1980).
[13] W. H. Wang, Prog. Mater. Sci. **52**, 540 (2007).
[14] W. Zhang, F. Jia, Q. Zhang, and A. Inoue, Mater. Sci. Eng. A **459**, 330 (2007).
[15] F. R. Niessen, *Cohesion in Metals* (Elsevier Science Publishers, Amsterdam, 1988), p. 224.
[16] E. A. Stern, M. Newville, B. Ravel, Y. Yacoby, and D. Haskel, Physica (Amsterdam) **208–209B**, 117 (1995).
[17] D. Vanderbilt, Phys. Rev. B **41**, 7892 (1990).
[18] F. Jia, W. Zhang, and A. Inoue, Mater. Trans., JIM **47**, 1922 (2006).
[19] L. E. Tanner and R. Ray, Scr. Metall. **11**, 783 (1977).
[20] M. C. Payne, M. P. Teter, D. C. Allan, T. A. Arias, and J. D. Joannopoulos, Rev. Mod. Phys. **64**, 1045 (1992).
[21] A. L. Ankudinov, B. Ravel, J. J. Rehr, and S. D. Conradson, Phys. Rev. B **58**, 7565 (1998).
[22] X. M. Huang, X. D. Wang, Y. He, Q. P. Cao, and J. Z. Jiang, Scr. Mater. **60**, 152 (2009).
[23] J. J. Rehr and R. C. Albers, Rev. Mod. Phys. **72**, 621 (2000).
[24] See EPAPS Document No. E-PRLTAO-103-026935 for supplementary material. For more information on EPAPS, see http://www.aip.org/pubservs/epaps.html.
[25] J. L. Finney, Proc. R. Soc. A **319**, 479 (1970).
[26] Z. P. Lu and C. T. Liu, Phys. Rev. Lett. **91**, 115505 (2003).
[27] P. I. Hurtodo, L. Berthier, and W. Kob, Phys. Rev. Lett. **98**, 135503 (2007).
[28] H. Shintani and H. Tanaka, Nature Phys. **2**, 200 (2006).
[29] P. H. Gaskell, Nature (London) **276**, 484 (1978).